第 33 卷第 12 期 焊 接 学 报 Vol. 33 No. 12
2012 年 12 月 TRANSACTIONS OF THE CHINA WELDING INSTITUTION December 2012

脉冲燃烧型立焊焊条

吴永胜， 王建江， 辛文彤， 刘浩东
(军械工程学院 先进材料研究所，石家庄 050003)

摘 要：介绍了一种用于战时野外应急抢修的新型手工自蔓延立焊焊条——脉冲燃烧型焊条. 首先分析普通手工自蔓延焊条(简称普通燃烧型焊条)实施立焊时存在的问题与不足，设计了脉冲燃烧型焊条，给出焊条结构与成分配比. 然后以低碳钢为焊接母材进行立焊试验，进行了 SEM，XRD 和 EDS 分析. 结果表明，焊缝由富铁相和富铜相组成，其中富铁相以 α-Fe 为主，含有少量的 FeNi，ε-Cu 和 $Cu_{0.81}Ni_{0.19}$；富铜相以 ε-Cu 为主，含有少量 $Cu_{0.81}Ni_{0.19}$，α-Fe 和 FeNi. 富铁相呈树枝晶状分布在富铜相基体上，焊缝合金与母材结合良好，达到单面焊双面成形. 焊接接头力学性能测试结果显示抗拉强度可达 367 MPa，焊缝合金区硬度 143.8 HV.

关键词：脉冲燃烧型焊条；立焊；组织性能
中图分类号：TG456.9 **文献标识码**：A **文章编号**：0253－360X(2012)12－0109－04

吴永胜

0 序 言

手工自蔓延焊接是一种新的自蔓延熔焊方法，该方法以燃烧型焊条为焊接材料，焊条自身燃烧合成反应产生的热量将焊接母材局部加热熔化，用反应的产物填充焊缝，采用焊条电弧焊的操作方法，实现焊接母材的永久牢固连接[1－4]. 手工自蔓延焊具有不需要外界能源和设备、携带使用安全方便、焊接操作灵活简单以及对金属表面锈蚀不敏感等显著的优点. 由于手工自蔓延焊作为一种特殊的熔焊技术，在热源、母材熔化、熔池特点、结晶机理等方面与普通熔焊存在着很大的区别，特别是在用普通手工自蔓延焊条进行立焊操作时，焊件的连接状况离满足野外应急抢修的要求还有一定差距，主要表现在(1)熔池凝固慢，在重力作用下的下淌严重；(2)焊缝上部焊件极易烧穿；(3)焊缝中极易形成夹渣. 因此针对立焊要求展开新的研究，研发新的焊接材料具有十分重要的意义.

1 脉冲燃烧型焊条结构与焊药成分设计

根据普通手工自蔓延焊条立焊过程中存在的问题，分析认为主要原因有(1)普通手工自蔓延焊条在焊接过程中燃烧所释放的热量过大且连续作用于焊件，导致熔池凝固慢而下淌严重；(2)熔融金属流失使焊件变薄，而普通手工自蔓延焊条的连续高热作用导致熔融金属持续流失最终致使焊件局部位置烧穿；(3)由于熔池凝固成形不规律，焊条燃烧产生的熔融焊料进入熔池后熔渣分离不及时，进而形成焊缝夹渣. 所以针对立焊所研究的焊接材料需适当降低热量，且热量供应要有利于熔池凝固成形.

根据以上分析设计研制一种新型燃烧型焊条——脉冲燃烧型焊条. 脉冲燃烧型焊条结构初步设计由高热焊药段和低热造渣段交替排列组成：高热焊药段燃烧时产生较大的热量，母材局部熔化形成熔池，焊药燃烧所生成的金属与熔池混合填充焊缝. 低热造渣段燃烧产生低热量仅能维持焊条燃烧，此时熔池冷却凝固. 低热造渣段燃烧产生的熔渣覆盖在焊缝表面，一方面托住熔池中熔融金属向下流失，一方面保护焊缝金属被空气氧化，熔渣覆盖焊缝合金基本不影响形成下一熔池和焊缝成形. 高热焊药段和低热造渣段燃烧速度以及伴随的冶金反应均不同而达到脉冲式燃烧的效果.

图 1a 是脉冲燃烧型焊条整体示意图. 图 1b 是脉冲燃烧型焊条剖面示意图. 其中 1 是引火线段，2，4，6 分别为不同长度的第一、第二和第三高热焊药段，3，5 是相同长度的低热造渣段，7 是堵头. 高热焊药段发生自蔓延反应产生的大量热量使母材局部熔化，形成熔池，而低热造渣段维持燃烧，不形成

收稿日期：2011－10－24

熔池，使焊条燃烧达到脉冲焊接效果.

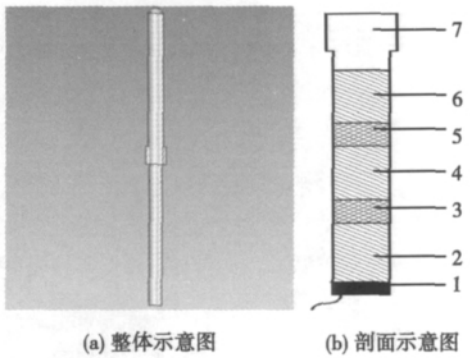

图 1 脉冲燃烧型焊条装配及焊条剖面图

Fig. 1 Scheme of assemblage and cross section for pulse combustion welding rod

2 试验方法与原理

脉冲燃烧型焊条外径 ϕ10 mm，长度 140 mm. 高热焊药段由高热剂、造渣剂、合金剂和脱氧剂组成，高热剂主要成分为 CuO，Fe_2O_3 和 Al，约占焊药(质量分数) 40% ~60%；造渣剂选自 $CaCO_3$，SiO_2，CuO，Fe_2O_3，CaF_2，$Na_2B_4O_7$，KNO_3 和 V_2O_5，约占焊药 20% ~25%；合金剂选自钼、镍及稀土材料，约占焊药 10% ~20%；脱氧剂选自铁、钛和锰，约占焊药 10% ~15%. 低热造渣段由高热剂、造渣剂和稀释剂组成，高热剂主要成分为 CuO，Fe_2O_3 和 Al，约占焊药 35% ~50%；造渣剂选自 $CaCO_3$，SiO_2，CaF_2，KNO_3 和 V_2O_5，约占焊药 35% ~45%；稀释剂选自 $Na_2B_4O_7$，TiO_2 和锰矿，约占焊药 15% ~20%. 把焊药混合均匀后按图 1 所示装入焊条即可得脉冲燃烧型焊条.

焊接试验采用板材对接立焊，运条方法类似焊条电弧焊，试验所用焊接母材为 Q235 钢板，尺寸为 70 mm × 40 mm × 3 mm，不开坡口，将母材不留间隙对接，不需要清理母材上的锈蚀. 焊接时用火柴点燃引火线，引火线段燃烧引燃焊药，焊药发生燃烧合成反应形成燃烧弧，采用焊条电弧焊的运条方法，高热焊药段反应产生的大量热量使母材局部熔化，形成熔池，冷却后生成的金属产物填充到焊缝中；低热造渣段热量过低无法形成熔池，生成的熔渣覆盖于金属焊缝之上.

依据国家标准 GB/T2649—1989、国家标准 GB/T2653—1989 和国家标准 GB/T3965—1995 中的相关规定，对焊接接头进行了拉伸性能试验，并且使用 XJL-17(4XC) 型金相显微镜、D8 Advance 型 X 射线衍射仪、Quanta-FEG 250 型扫描电镜和 INCA 型能谱仪进行焊接接头的组织分析.

3 试验结果

焊接结束，焊件完全冷却后，轻轻敲打即可除去焊缝表面熔渣，焊接接头完整，焊缝表面成波浪形，质量良好无表面裂纹. 图 2 所示为焊缝正面宏观形貌，由图 2 可见，焊道宽度均匀，焊缝呈金属光泽. 图 3 所示为焊缝背面宏观形貌，母材沿焊缝焊透，基本达到单面焊双面成形的效果.

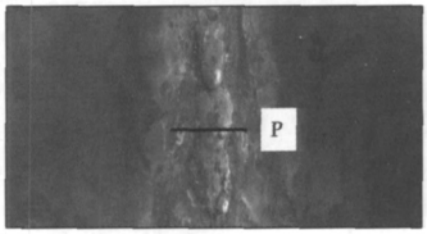

图 2 焊缝正面宏观形貌

Fig. 2 Appearance of front of welding seam

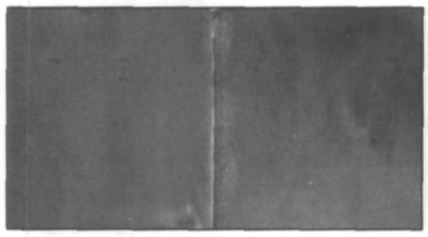

图 3 焊缝背面宏观形貌

Fig. 3 Appearance of back of welding seam

对焊接试样进行力学性能测试，抗拉强度可达 367 MPa，在焊缝区断裂，断口未见明显缺陷. 如图 2 中所示 P 处截取试样，按照图 4 所示，每隔 0.5 mm 测一个硬度值，共测得 5 个点取平均值，分别测试了焊缝合金区和热影响区硬度值，测得数据如表 1 所示. 由力学性能测试数据可以看出，焊接接头中焊缝合金区相对较为薄弱，故重点分析焊缝合金区组织.

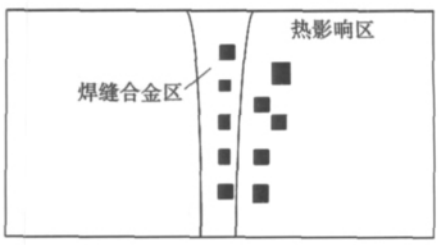

图 4 焊接接头显微硬度测试方法示意图

Fig. 4 Method of micro-hardness test in welding joint

表 1　焊接接头显微硬度测试结果(HV)

Table 1　Micro-hardness value of welding joint

测试点	焊缝合金区硬度值	热影响区硬度值
1	148.3	158.2
2	137.5	164.3
3	140.7	168.1
4	142.9	163.9
5	149.4	170.6
平均值	143.8	165.0

4　分析与讨论

图 2 中所示 P 处截取试样进行组织分析. 图 5 为焊缝金相显微组织形貌,由图 5a 可以看出焊缝整体形成,深色区域为母材,浅色为焊缝合金; 由图 5b 可以看出焊缝中组织分布均匀,基本没有明显缺陷. 图 6 为焊缝 SEM 形貌及不同组织 EDS 分析,结果显示焊接获得的焊缝合金为铜铁镍合金,主要合金元素有 Fe,Cu,Ni,还有少量 C,Si. 图 6 中 A 点成分主要为 Fe 元素,B 点成分主要为 Cu 元素,对应图 5 中浅色基体为富铜相,深色析出部分为富铁相,富铁相形成的树枝晶均匀分布在富铜相内. 有研究指出铜铁混合熔体的互溶度依赖于熔液中杂质元素,尤其是 C,Si,Ni,Pb 和 Zn 等元素[5,6],但是 C 元素含量超过 0.2% 熔液凝固会出现显著的铜铁液相分离,且绝大部分 C 元素在富铁相中出现[7]. EDS 分析结果显示 A 点中 C 和 Si 等元素含量比 B 点高,与以上研究结果基本一致. 对试样进一步 XRD 物相分析如图 7 所示,测试结果显示,焊缝中的金属元素 Cu,Fe,Ni 主要以 α-Fe,ε-Cu,FeNi 和 $Cu_{0.81}Ni_{0.19}$ 存在. 结合 EDS 分析可以确定富铁相以 α-Fe 为主,含有少量的 FeNi,ε-Cu 和 $Cu_{0.81}Ni_{0.19}$; 富铜相以 ε-Cu 为主,含有少量 $Cu_{0.81}Ni_{0.19}$,α-Fe 和 FeNi.

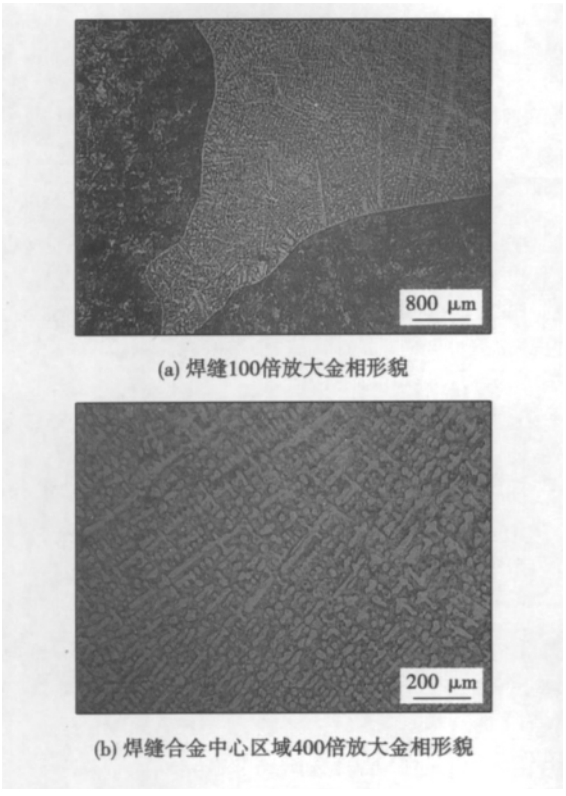

图 5　焊缝金相显微组织

Fig. 5　Metallographic microstructure of welding seam

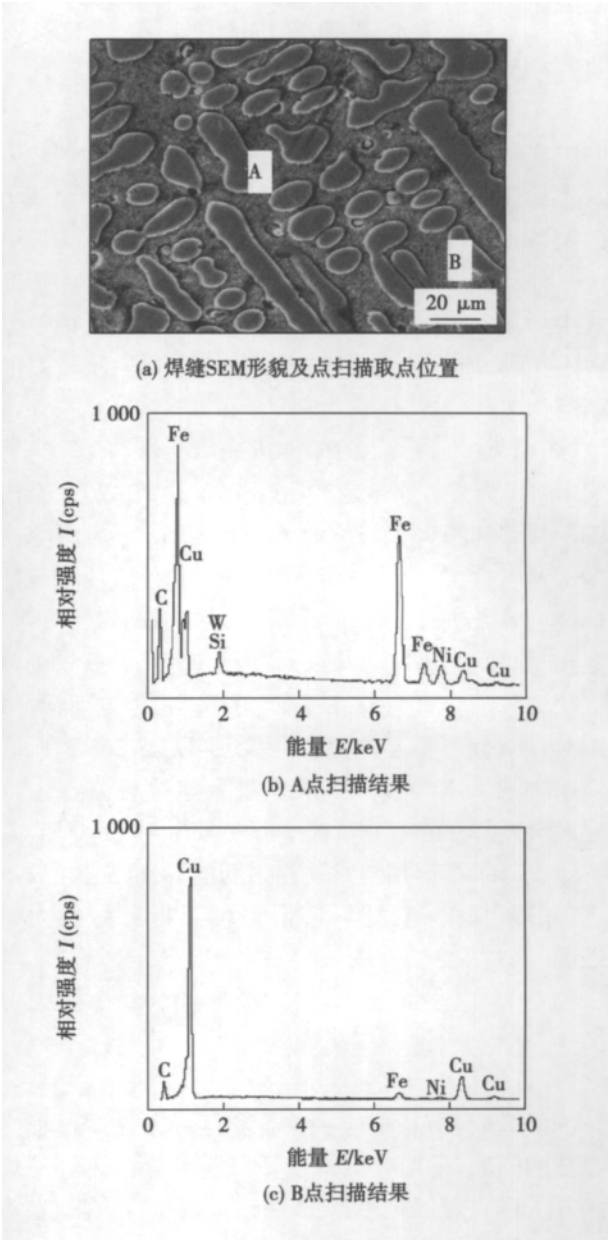

图 6　焊缝 SEM 形貌及点成分分析

Fig. 6　SEM and EDS of welding seam

由于树枝晶的枝臂间距关系着溶质和杂质的分布以及亚晶粒的粗细,故枝臂间距大小对材料的力学性能影响很大. 枝臂间距愈小,力学性能愈高,强度和断后伸长率可得到显著改善[8]. 一次枝晶的

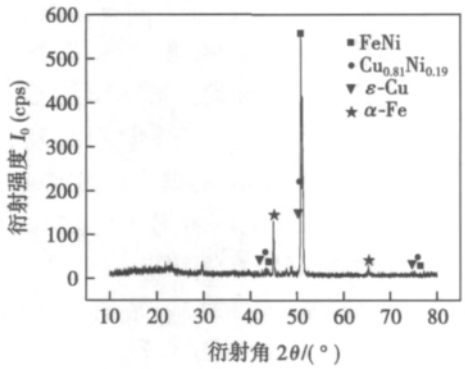

图 7 焊缝 XRD 分析图谱

Fig. 7 XRD patterns of welding seam

间距 λ_1 以及二次枝晶的间距 λ_2 都和温度梯度 G_L 及生长速率 R 有密切关系，一般认为 λ_1 和 G_L 与 R 的关系为[9,10]

$$\lambda_1 = A_L G_L^{-m} R^{-n} \quad (1)$$

式中：A_L，m 和 n 都是常数. 不同研究者提供的数据各不相同，有人认为 $m \approx 0.5$，$n \approx 0.25$. 二次枝晶的间距为

$$\lambda_2 = B_L (G_L R)^{-n} \quad (2)$$

式中：B_L 为常数；$n \approx 1/3$. 由式(1)，式(2)可以看出影响枝臂间距大小的主要因素是 $G_L R$(冷却速度)，冷却速度愈大，分枝愈多，枝臂间距愈小. 使用脉冲燃烧型焊条进行立焊试验，熔池加热时间短，焊后熔池在短时间内迅速冷却成形，冷却速度大，获得的富铁相树枝晶分布均匀，枝臂间距小. 另一方面，焊缝中 Cu，Fe 元素不互溶，凝固后以 α-Fe，ε-Cu 存在，在焊条中加入 Ni 元素，Ni 元素进入熔池后，与 Cu，Fe 元素均可无限互溶，在试验中形成 FeNi 和 $Cu_{0.81}Ni_{0.19}$，有效改善了富铜相与富铁相之间的界面结合. 故虽然焊缝基体为铜固溶体，但仍可获得良好的力学性能.

5 结 论

(1) 研究分析普通手工自蔓延焊条立焊过程中存在的问题，采用分段式设计研制了脉冲燃烧型焊条并进行立焊试验，结果表明该方法可行，焊接基本达到预期效果.

(2) 高热焊药段使母材局部熔化形成焊缝，低热造渣段辅助焊缝成形并保护焊缝，最终形成良好焊缝，达到单面焊双面成形的效果.

(3) 焊接获得的焊缝合金为铜铁镍合金，铜基体与析出富铁相分布均匀，富铁相树枝晶枝臂间距小；Ni 元素的加入形成 FeNi 和 $Cu_{0.81}Ni_{0.19}$ 改善了富铜相与富铁相之间的界面结合，焊缝力学性能高，抗拉强度可达 367 MPa，焊缝合金硬度 143.8 HV.

参考文献：

[1] 辛文彤，李志尊，李宝峰，等. 一种野外快速焊接技术[J]. 焊接，2005(1)：19－21.
Xin Wentong，Li Zhizun，Li Baofeng，*et al*. Study on quick welding technology under field operations circumstances [J]. Welding & Joining，2005(1)：19－21

[2] 李志尊，辛文彤，武 斌，等. 高热剂对低碳钢手工自蔓延焊接的影响[J]. 焊接学报，2007，28(2)：79－81.
Li Zhizun，Xin Wentong，Wu Bin，*et al*. Effect of thermit composition on manual SHS welding for low carbon steel [J]. Transactions of the China Welding Institution，2007，28(2)：79－81.

[3] 辛文彤，马世宁，李志尊，等. Fe 基手工自蔓延焊接接头的组织和性能[J]. 焊接学报，2009，30(10)：73－75.
Xin Wentong，Ma Shining，Li Zhizun，*et al*. Structure and property of Fe-base manual SHS welding joint [J]. Transactions of the China Welding Institution，2009，30(10)：73－75.

[4] 辛文彤，马世宁，李志尊，等. 焊后热处理对手工自蔓延焊接接头组织性能的影响[J]. 焊接学报，2009，30(6)：83－86.
Xin Wentong，Ma Shining，Li Zhizun，*et al*. Effect of post-weld heat treatment on microstructure and mechanical property of manual SHS welding [J]. Transactions of the China Welding Institution，2009，30(6)：83－86.

[5] Maddocks W R. Claussen C E. Part-III the Fe-Cu-Co system [J]. Iron Steel Institute，1936(14)：97－124.

[6] Iwase K，Okamoto M. Amemiya T. On the formation of two liquid layers in copper-iron alloys [J]. Tohoku Imperial University，1938(26)：618－628.

[7] Smith C S，Palmer E W. Undercooling of minor liquid in binary alloys [J]. Metallurgical and Materials Transactions AIME，1950(188)：1486－1499.

[8] 刘智恩. 材料科学基础[M]. 2 版. 西安：西北工业大学出版社，2003.

[9] Minkoff I. Solicitation and cast structures [M]. New York：John Wiley & Sons Limited，1986.

[10] 余永宁. 金属学原理[M]. 北京：冶金工业出版社，2010.

作者简介：吴永胜，男，1985 年出生，博士研究生. 主要从事自蔓延焊接技术研究与应用工作. 发表论文 6 篇. Email：wuysh.2007@163.com

通讯作者：王建江，男，教授. Email：JJWang63@heinfo.net

MAIN TOPICS, ABSTRACTS & KEY WORDS

Nonlinear gradient features of grain size in TIG welded joint for titanium alloy ZHANG Jianxun[1], DONG Lina[1], ZHANG Linjie[1], WANG Yiqing[2] (1. State Key Laboratory for Mechanical Behavior of Materials, Xi'an Jiaotong University, Xi'an 710049, China; 2. School of Mechanical Engineering, Xi'an Jiaotong University, Xi'an 710049, China). pp 1 – 4

Abstract: In the paper, based on the grain size observation and statistics analysis on TIG welded joints of TC4 titanium alloy, the gradient features of the gain sizes in welded joints with different heat input are studied experimentally for characterizing the microstructure heterogeneity by introducing a conception of grain gradient eigenvalue. The results show that the grain size in the TIG welded joint nonlinearly changes from the center of weld metal after the heat affected zone to the base metal, and the size changing rate (grain gradient) has a maximum value in the boundary between the columnar zone (CZ) and coarse grain zone (CGZ). The grain size gradient maximum value proposed as the grain gradient eigenvalue is inversely proportional to heat input in TIG welding and its position is independent with the heat input. The concept of the gain gradient eigenvalue can represent the microstructure heterogeneity in the welded zone and heat affected zone, and is significantly important for evaluating the service properties of titanium alloy welded joint.

Key words: titanium alloy; TIG welding; grain size

Interfacial structure and strength of Si_3N_4 ceramics joint brazed with amorphous filler metal and Cu layer ZOU Jiasheng, ZUO Huaiwen, XU Xiangping (Provincial Key Lab of Advanced Welding Technology, Jiangsu University of Science and Technology, Zhenjiang 212003, China). pp 5 – 8

Abstract: Si_3N_4 ceramics were brazed with TiZrCuB amorphous filler metal and Cu interlayer, the effect of brazing metal compositions and thickness of copper foil on interfacial structure and bonding strength were studied in this paper. The result shows that the joint strength is up to 241 MPa when the brazing temperature is 1 323 K, holding time is 30 min, the thickness of Cu interlayer is 70 μm and the exerted pressure is 0.027 MPa. The reaction layer is TiN and the interface microstructure is compound of Si_3N_4/TiN/Ti-Si + Ti-Zr + Cu-Zr + α-Cu. Changing the thickness of interlayer can adjust the thickness and compositions of the reaction layer. As the thickness of Cu interlayer increased, Ti-Si compound layer was gradually separated from the TiN layer, and was pushed into the weld center and refined to a granular shape.

Key words: amorphous brazing filler metals; Cu interlayer; Si_3N_4 ceramics; interface structure; bending strength

Task planning and simulation of two-robot welding coordination ZHANG Tie, OUYANG Fan (School of Mechanical & Automotive Engineering, South China University of Technology, Guangzhou 510640, China). pp 9 – 12

Abstract: This paper focuses on the dual-robot welding coordination of complex curve seams that one robot grasps the workpiece while the other holds the torch, then the two robots work on the same workpiece coordinately. The dual-robot coordination system is established at the beginning, after that, the non master/slave scheme is chosen for the kinematics trajectory planning. The non master/slave scheme sets the position and poses of the point on the workpiece, and calculates the end effecter trajectories of both robots through the constrained matrixes respectively. Downhand welding is employed in the kinematics trajectory planning that can guarantee the torch and the weld in good contact condition all the time during the welding process. Moreover, a Solidworks-SimMechanics platform is established for motion simulation, and an example of curved steel pipe welding is conducted. The results indicate that the established platform is accurate and effective for the task planning and analysis welding coordination of two robots. The output trajectories of both the joint displacements and end effectors are the same as predefined ones.

Key words: complex curve seam; two robot; coordination of welding

Study on influence factors of temperature in localized ultra-high frequency induction brazing SU Honghua, LI Qilin, XU Jiuhua, FU Yucan (College of Mechanical and Electrical Engineering, Nanjing University of Aeronautics & Astronautics, Nanjing 210016, China). pp 13 – 17

Abstract: The technology of localized ultra-high frequency induction brazing is introduced. The effect of influence factors, such as material of ferrite core, gap and coil structure, on temperature in induction brazing are investigated and analyzed. An optimal combination of technological parameters is obtained through experiments. At last, localized ultra-high frequency induction brazing of diamond is carried out based on the above parameters. The result demonstrates that the width of melted area of filler alloy is less than 3 mm. The diamond is wetted by the filler alloy. The interfacial structure between diamond and filler alloy is investigated by scanning electron microscope (SEM) and energy dispersion spectrometer (EDS). The result shows that the bond between diamond and filler alloy is established through a cross-diffusion of carbon and chromium.

Key words: diamond; localized heating; ultra-high frequency; induction brazing

Microstructure and corrosion resistance of welding joints of economic ferritic stainless steel ZHANG Yong[1], QIN Zuoxiang[1], XU Hongji[1], LU Xing[1], TONG Wei[2] (1. Liaoning Key Materials Laboratory for Railway, Dalian Jiaotong University, Dalian 116028, China; 2. School of Transport and Communication Engineering, Dalian Jiaotong University, Dalian 116028, China). pp 18 – 22

Abstract: TCS345, T4003, Nirosta 4003 and JFE410RW ferritic stainless steels were welded by ER-309 welding wire in this paper. The microstructure of their base metal and joint were analyzed by metallographic approach, and the corrosion resistance of base metal and joints was evaluated by electrochemical corrosion tests. The experimental results demonstrated that, compared with that of Nirosta 4003 and JFE410RW, low content of Ti and Mn elements were found in TCS345 and T4003 ferritic stainless steels, especially the low content of Ti, which resulted in the obvious grain growth of TCS345 and T4003 ferritic stainless steels. Moreover, the welding joints of ferritic stainless steels exhibited big heat affected zone (HAZ). Compared with the microstructure of base metal, the HAZ area showed obvious large grains. As far as TCS345 is concerned, obvious grain growth is observed. In the case of Nirosta 4003 and JFE410RW, they exhibited smaller size of grain than TCS345. In 1mol/L Na_2SO_4 solution, the corrosion resistance of TCS345 and JFE410RW is better than that of T4003 and Nirosta 4003.

Key words: ferritic stainless steel; welding joint; metallographic microstructure; corrosion resistance

Effect of microplasma spraying working gas on crystallinity of HA coatings ZHAO Qiuying[1], HE Dingyong[2], LIU Yan[2], LI Xiaoyan[2], CHEN Shujun[3] (1. Postdoctoral Research Station of Mechanical Engineering, Beijing University of Technology, Beijing 100124, China; 2. College of Materials Science and Engineering, Beijing University of Technology, Beijing 100124, China; 3. College of Mechanical Engineering and Applied Electronics Technology, Beijing University of Technology, Beijing 100124, China). pp 23 - 27

Abstract: Hydroxyapatite (HA) coatings were prepared on Ti-6Al-4V substrate by using the method of microplasma spraying. Commercially pure argon gas and helium/argon (50% in volume) mixed gas were used as working gas in the spraying processing respectively. The surface morphology, phase compositions and degree of crystallinity of the coatings were examined by scanning electron microscope (SEM) and X-ray diffraction (XRD). Results show that less impurity phases and no TTCP and CaO phases were found in the coatings. The crystallinity of coatings is higher than 70%, which is beneficial for implantation materials stability in vitro and vivo. The enthalpy of microplasma arc in which helium/argon mixed is used as working gas is higher than that in which commercially pure argon gas is used. The crystalline phases in the former coatings mainly consist of recrystallization grains while the latter coatings were mainly made up of lots of unmelted HA particles.

Key words: microplasma spraying; hydroxyapatite coatings; helium/argon mixed gas; crystallinity

Development of hybrid laser + double wire MIG/MAG welding system and process ZHU Yanli[1], LI Huan[1], YANG Lijun[1], GAO Ying[2] (1. Tianjin Key Laboratory of Advanced Joining Technology, Tianjin University, Tianjin 300072, China; 2. Tianjin Key Laboratory of High Speed Cutting and Precision Machining, Tianjin University of Technology and Education, Tianjin 300222, China). pp 28 - 32

Abstract: In order to study the process of laser + double wire welding, the hybrid laser + double wire MIG/MAG welding system was constructed. The method of pulsed controlling of the powers which are mutually independent is alternative. The welding experiments were also carried out with this system in this paper. The double current signals, voltage signals and high-speed camera signals were synchronously collected. The result shows that the hybrid laser + double wire MIG/MAG welding system can carry out stable welding and the appearance of the weld is good. The diversifications of voltage signals were obvious and the stability of voltage signals was improved as a result of injection of the laser power.

Key words: hybrid laser + double wire MIG/MAG welding; electric signals; high-speed camera

Effect of TGO topography on TBCs residual stresses HAN Zhiyong, ZHANG Hua, WANG Zhiping (Tianjin Key Laboratory for Civil Aircraft Airworthiness and Maintenance, Civil Aviation University of China, Tianjin 300300, China). pp 33 - 36

Abstract: By using nonlinear finite element model, the residual stress distribution which was affected by interface topography of top ceramic coat (TCC), bond coat (BC) and thermally-growth oxide (TGO) interface area in thermal barrier coatings (TBCs) system was calculated. In the process of calculation, thermodynamic parameters of TCC, TGO and BC were considered. The calculating results show that the residual stress of TGO interface is affected by interface topography unit size and topography distribution density obviously. The stress on TCC/TGO interface is greater than that on BC/TGO interface. Stress concentrates at the tip of cone topography center and reaches the maximum value, which becomes the dangerous point for failure of thermal barrier coatings system. The residual stress level decreases with the increasing of topography quantity.

Key words: thermal barrier coatings; nonlinear calculation; interface topography; TGO

Study on performance of 6156 skin butt joint with laser beam welding ZHAN Xiaohong[1,2], CHEN Jie[1], TAO Wang[3], YANG Zhibin[3], WEI Yanhong[2,3], CHEN Yanbin[3], OU Wenmin[2] (1. Shanghai Aircraft Manufacturing Co., Ltd, Shanghai 200436, China; 2. College of Material Science and Technology, Nanjing University of Aeronautics and Astronautics, Nanjing 210016, China; 3. State Key Laboratory of Advanced Welding Production Technology, Harbin Institute of Technology, Harbin 150001, China). pp 37 - 40

Abstract: The laser beam welding characteristics of 6156 aluminum butt joint with and without filling wire are investigated. The factors which influence the weld appearance and weld width are analyzed. The variety rule of tensile and fatigue strength are discussed. The results show that the appearance of the weld joint with filler metal is better than the one without filler metal. The maximum weld gap tolerance of the weld joint with filler metal increases to 0.7 mm. The strength of weld joint without heat treatment is 314.3 MPa which is 81.3% of base metal. Laser welding of aluminum is a favorable weld technology with the characteristics of high speed, fine weld appearance and wide weldability.

Key words: laser beam welding; aluminum alloy; butt

joint; filling weld

Analysis and prevention of cracks in laser-welded joint of TiNi shape memory alloy and stainless steel LI Hongmei[1], SUN Daqian[1], DONG Peng[1], CAI Xiaolong[2] (1. School of Materials Science and Engineering, Jilin University, Changchun 130025, China; 2. State Key Laboratory of Rare Earth Resources Utilization, Changchun Institute of Applied Chemistry, Changchun 130022, China). pp 41 - 44

Abstract: Dissimilar metal joints of TiNi shape memory alloy wire and stainless steel wire were welded by laser welding method. The cracks feature and fracture surface morphology of joints were examined by using scanning electron microscopy (SEM) and confocal laser scanning microscope (CLSM). The mechanism of crack formation were analyzed, and some measurements were taken to control the welding cracks. The results showed that the micro-cracks usually emerged in the center of the weld zone and fusion zone of TiNi alloy side. The existence of a large number of brittle compounds in the weld was internal cause of cracks, and the joint subjected to tensile stress was the necessary condition of cracks. The cracking susceptibility can be improved to a certain extent by adding Ni interlayer, Co interlayer, changing the laser beam position, applying an axial force to weld zone and optimizing the laser welding parameters. Adding metal interlayer was a more effective method. The tensile strength reached 372 MPa and 347 MPa respectively by using Ni and Co interlayer, and the joint strength increased by 98.9% and 85.6% respectively, compared with the joint without metal interlayer.

Key words: TiNi shape memory alloy wire; stainless steel wire; laser welding; cracks

Experimental analysis on fusion ratio and composition uniformity of laser hot wire welds ZHENG Shiqing[1], WEN Peng[1,2], SHAN Jiguo[1,2] (1. Department of Mechanical Engineering, Tsinghua University, Beijing 100084, China; 2. Key Lab for Advanced Materials Processing Technology, Ministry of Education, Beijing 100084, China). pp 45 - 48, 72

Abstract: Ductile cast iron is welded with filling stainless steel hot wire in this article, then fusion ratio and distribution of elements are studied. The fusion ratio is as low as 38%-55%. The composition of filler wire distributes in welds uniformly. Nonuniform degrees of element Cr and Ni are 0.5% and 6%. Compared with laser hot wire welding, the fusion ratio of laser-MIG hybrid welds is 69%-77%, and the nonuniform degrees of element Cr and Ni are not less than 62% and 51%. The low electric energy input and its high utilization ratio for heating filler wire contribute to lower fusion ratio in laser hot wire welding compared to laser-MIG hybrid welding. The uniform distribution of filler wire in laser hot wire welds results from the low fusion ratio and solid filler wire transfer.

Key words: laser hot wire welding; laser-MIG hybrid welding; fusion ratio; distribution of elements; ductile cast iron

Joint microstructure and isothermal solidification modeling during transient liquid-phase bonding of a duplex stainless steel YUAN Xinjian[1], LUO Jun[1], TANG Kunlun[1], LI Jia[1], KANG Chungyun[2] (1. College of Materials Science and Engineering, Chongqing University, Chongqing 400044, China; 2. Department of Materials Science and Engineering, Pusan National University, Busan 609735, Korea). pp 49 - 52

Abstract: An experimental investigation on transient liquid-phase bonding of a duplex stainless steel was carried by using Ni-based amorphous alloy as the interlayer. The microstructure of the bonded joint was observed with field emission scanning electron microscope (FE-SEM). The chemical compositions were analyzed by energy-dispersive X-ray spectroscopy (EDS) and wavelength-dispersive spectrometry (WDS). Phase structure of the bonded joint was identified by using X-ray diffraction (XRD). The results indicated that before the completion of isothermal solidification, the major secondary-phase precipitate present in the interface region between the insert and base alloy was BN. The dominating phases appeared in the interlayer zone were γ-Ni solid solution, Ni_3B and Cr-borides. Additionally, three diffusion models were employed to calculate the completion time of the isothermal solidification. By contrast to experimental results, the value obtained by solute distribution model was close to the actual value, and this model was considered to be suitable to the bonding process.

Key words: duplex stainless steel; Ni-based amorphous alloy; transient liquid-phase; microstructure; isothermal solidification

Affecting factors of forming spiking of titanium alloy electron beam deep penetration welding SHI Mingxiao[1], ZHANG Binggang[2], MA Jilong[2], CHEN Guoqing[2], FENG Jicai[2], FAN Ding[1] (1. State Key Laboratory of Gansu Advanced Non-ferrous Metal Materials, Lanzhou University of Technology, Lanzhou 730050, China; 2. State Key Laboratory of Advanced Welding and Joining, Harbin Institute of Technology, Harbin 150001, China). pp 53 - 56

Abstract: The spiking is the unique defect of electron beam welding, which has a serious impact on the welding quality. The academia still hadn't had an unified understanding of the forming mechanism of spiking. To study the forming mechanism of spiking, the orthogonal test was used to carry out the experiment of titanium alloy electron-beam deep-penetration welding. The X-ray detection was done for each weld after welding The results of X-ray detection show that the spiking only exists in the partial penetration weld, and the spiking is the irregular-slited shape while the roots are round. The optical microscope and scanning electron microscope combined with energy dispersion spectroscopy were used to analyze the formation mechanism of spiking. The results show that the pulse of electron beam is the direct cause of spiking formation and the metal vapor with high saturated vapor pressure accelerates the tendency of forming spiking. It is important intrinsic motivation to the generation of spiking.

Key words: electron beam welding; metal vapor; spiking

Effect of trace calcium on performance of AgCuZn alloy BAO Li[1], LONG Weimin[1], ZHANG Guanxing[1], SUI Fangfei[2], LI Hao[2], MA Jia[2] (1. State Key Laboratory of Advanced Brazing Filler Metals and Technology, Zhengzhou Institute of

Mechanical Engineering, Zhengzhou 450001, China; 2. School of Material Science and Engineering, Zhengzhou University, Zhengzhou 450001, China). pp 57 - 60

Abstract: The purity of the brazing alloys is necessary to be improved with the increasing cleanness of steel. This paper aims at investigating the influence of trace calcium that is contained in filler metal during production process. The melting property, microstructure and spreading performance of BAg45Cu30Zn alloy with various calcium additions have been studied, by employing simultaneous thermal analyzer and scanning electron microscope. The results show that the solidus temperature increases, the liquidus temperature decreases and the melting range narrows, with the calcium content increasing in alloy. The element calcium in the form of CaO exists as the crystal nucleus to refine alloy microstructure. The spreading performance of alloy on 316LN stainless steel has been weakened, resulting from the existence of calcium element.

Key words: trace calcium; AgCuZn brazing alloy; melting property; microstructure; spreading performance

Microstructure and mechanical behaviors of stainless steel weld metal by ultrasonic assisted pulse TIG welding technology ZHANG Qinlian, LIN Sanbao, FAN Chenglei, YANG Chunli (State Key Laboratory of Advanced Welding and Joining, Harbin Institute of Technology, Harbin 150001, China). pp 61 - 64

Abstract: Ultrasonic assisted TIG welding is a new technology with high efficiency. In previous study, direct current was used. However, pulse current was expected in actual welding production. In this study, ultrasonic assisted pulse TIG welding technology was applied to weld 1Cr18Ni9Ti austenitic stainless steel. Microstructure and mechanical properties of the joints were analyzed. The reasons for weld penetration increasing and microstructure refinement were discussed. Experimental results indicated that the welding penetration with ultrasonic vibration was double of that without it. The microstructure of the weld zone was refined and the arc shape was compressed in base current period. The ultimate tensile strength and elongation were higher than that without ultrasonic vibration. Weld penetration increasing is perhaps attributed to acoustic streaming as the main driving force. The refinement of microstructure may be caused by the corporate effects of acoustic cavitation and acoustic streaming.

Key words: stainless steel; ultrasonic vibration; grain refinement; mechanical property

Study on life-prediction of solder joint under combined loading WANG Huan, YANG Ping, XIE Fangwei, XI Tao (School of Mechanical Engineering, Jiangsu University, Zhenjiang 212013, China). pp 65 - 68

Abstract: A life-prediction approach of solder joints under combined thermal and vibration loading is provided in this paper. The deformations of solder joints are calculated respectively under vibration and thermal cycling loading based on finite element method. The calculated results are defined as boundary conditions of the multiaxial loading to investigate the strain/stress of the solder joints. Then the life of solder joints is calculated. The result reveals that the life of solder joints can be divided into three regions according to the vibration amplitude at the same temperature: the life of solder joints in region Ⅰ is affected by thermal loading; that in region Ⅱ is greatly affected by the combined loading; that in region Ⅲ is affected by the vibration amplitude. The trend of the simulation results basically agrees with that of the test results.

Key words: solder joints; combined loading; life-prediction

Analysis for microstructure and mechanical property of Sn-3Ag-0.5Cu solder joints in high density LED packages WANG Xinxin[1], LIU Jianping[1], GUO Fu[1], LIU Li[2], LEI Yuanhong[2] (1. College of Materials Science and Engineering, Beijing University of Technology, Beijing 100124, China; 2. R&D Center, Beijing Leyard Electronic Science Technology Co., Ltd, Beijing 100091, China). pp 69 - 72

Abstract: The microstructure of Sn37Pb and Sn3Ag0.5Cu solder joints under as-reflowed and isothermal aged conditions were observed respectively. The shear strength of samples were also measured. The results suggested that despite the IMC layer of the Sn37Pb solder joints was thicker than the Sn3Ag0.5Cu solder joints, both of them were within the acceptable range. The Sn3Ag0.5Cu solder joints shows a bigger shear strength due to its special structure of β-Sn primary crystal coated by reticular eutectic. Besides, the shear strength of the two solder joints decreased after aging. Although lead-free solder is the inevitable trend to the development of electronic packaging industry instead of Sn37Pb solder, precision reflowing process still plays an important role to improve the quality of the solder joints.

Key words: LED package; eutectic solder alloys; microstructure; shear strength

Spectrum analysis of A-TIG welding for aluminum alloy YAN Keng[1], YANG Gang[1], ZHAO Yong[1], GAO Lihua[1], LU Jiansheng[2] (1. Provincial Key Lab of Advanced Welding Technology, Jiangsu University of Science Technology, Zhenjiang 212003, China; 2. Shanghai Waigaoqiao Shipbuilding Co., Ltd, Shanghai 200137, China). pp 73 - 76, 105

Abstract: A-TIG welding experiments were conducted by using five species of single-component activating fluxes, including SiO_2, TiO_2, CaF_2, Cr_2O_3, $BaCl_2$ and complex formulation YG304. The spectrum in A-TIG welding process is tested by spectrometer. The distribution law of flux element in arc space is analyzed. The experimental results indicate that the above activating fluxes have different effects on weld penetration. The most remarkable increasing is obtained when the flux is YG304. The spectral lines of argon atom and aluminum atom are the main spectral lines of the A-TIG welding arc. Different cross-spectrum distribution of arc is presented with different fluxes. The increasing of penetration may be attributed to the recombination of positive ions such as Si^{4+}, Ti^{4+}, Cr^{3+} and electron that generates from Ar arc, thus raise the arc temperature and arc force, and ultimately the weld penetration increases. The effect of increased penetration is due to various physical properties of positive ion.

Key words: aluminum alloy; A-TIG; cross-spectrum; weld penetration

Abstract: Based on the section analysis of three-dimensional model of friction stir welding, the evolution of the joint section of the welding process was established. The forming process of friction stir welding was divided into extrusion stage, migration stage, backfilling stage and shoulder effect stage. The first three stages which were affected by stir pin were analyzed. The analysis of the material migration processes of the first three stages pointed out that the original surface and the residual oxides were migrated to the retreat side in the extrusion stage, the onion ring structure was formed, the oxides were fragmentated and dispersed in the migration stage and the onion ring structure was fully formed in the backfilling stage. The studies showed that if the above three stages could not effectively complete the forming processes, the superposition effect of a variety of defects forming mechanisms would lead to the formation of the final defects. The results show that the four stages of the forming process established by using the section analysis can be used to explain the forming mechanisms of FSW joints and the causes of the "S line" and other defects.

Key words: friction stir welding; section analysis; joint forming; defect

Effects of welding heat source parameters on residual stress and distortion in thin plate joint WANG Nengqing, TONG Yangang, DENG Dean (College of Materials Science and Engineering, Chongqing University, Chongqing 400045, China). pp 97 – 100

Abstract: The thermo-elastic-plastic finite element method (FEM) has been widely used to predict temperature field, residual stress distribution and deformation. However, how to choose the parameters of moving heat source model for given welding conditions heavily depends on a analyst's experience. It is necessary to clarify the influence of heat source parameters on residual stress and deformation. Therefore, an attempt was made to examine the influence of heat source parameters on residual stress and deformation in a thin plate joint using thermo-elastic-plastic FEM with Goldak heat source model in the current work. The simulation results show that the heat source parameters have no significant effect on residual stress, but have effect on welding deformation to some extent.

Key words: heat source; welding residual stress; welding deformation; numerical simulation

Effects of laser shock wave on salt spray corrosion of X70 pipeline steel welded lines WU Yongzhong, KONG Dejun, LONG Dan, FU Guizhong (College of Mechanical Engineering, Changzhou University, Changzhou 213016, China). pp 101 – 105

Abstract: The surface of X70 pipeline steel welded line was treated by laser shock wave, and the corrosion performances before and after laser shock processing were analyzed by salt spray corrosion test in artificial atmosphere. The surface morphologies, chemical elements and phase constituent were observed with SEM (scanning electron microscope), EDS (energy dispersive spectrometer) and XRD (X-ray diffraction), respectively, and the effects of laser shock processing on the corrosion mechanism were discussed. The results show that tensile residual stress exists in the surface of X70 pipeline steel welded lines in primitive state, which improves stress corrosion crack with the interaction of corrosive medium Cl^-. Spelling corrosion occurs with the interaction of boundary corrosion. The grain refinements are produced in the welded lines by laser shock processing, and the strengthened layer is formed on the surface, which improves corrosion resistance of the welded lines.

Key words: laser shock processing; X70 pipeline steel; welded line; salt spray corrosion

Characteristics of Ni-Cr-Co-W-Mo-Ta-B brazing filler LI Wen[1,2], JIN Tao[2] (1. College of Materials Science and Engineering, Shenyang Ligong University, Shenyang 110159, China; 2. Institute of Metal Research, Chinese Academy of Sciences, Shenyang 110016, China). pp 106 – 108

Abstract: Ni-Cr-Co-W-Mo-B alloy powder was prepared by gas atomization. The particle morphology and element distribution of the powder were investigated by SEM. The melting characteristics of the Ni-Cr-Co-W-Mo-Ta-B powder were evaluated by DSC. The Ni-Cr-Co-W-Mo-Ta-B flexible insert alloy cloth was obtained through a thermal rolling technology. The bonding strength at room temperature and stress rupture life at 1 010 ℃/248 MPa were measured. The results indicate that Ni-Cr-Co-W-Mo-Ta-B particles existas ball-shape and the element distributions are homogeneous in the particles. The liquidus temperature of the alloy is 1 127 ℃. The tensile strength at room temperature and stress rupture life at 1 010 ℃/248 MPa of the completed joints are almost identical to those of the superalloy substrate when the Ni-base superalloy was bonded by the transient liquid phase (TLP) bonding using Ni-Cr-Co-W-Mo-Ta-B powder as an insert alloy.

Key words: Ni-Cr-Co-W-Mo-Ta-B powder; Ni-base superalloy; TLP bonding; mechanical properties

Study of pulse combustion welding rod for vertical weld WU Yongsheng, WANG Jianjiang, XIN Wentong, LIU Haodong (The Institute of Advanced Materials, Ordnance Engineering College, Shijiazhuang 050003, China). pp 109 – 112

Abstract: A new type of manual SHS welding rod called the pulse combustion rod is introduced, which is used in the urgent repair of war. Firstly, the problems and insufficiency of the normal manual SHS welding rod (normal combustion rod for short) are analyzed in the vertical weld. The pulse combustion rod is designed with structure and constitution presented. Then vertical weld experiment is carried out, in which low carbon steel is used as the base metal. By analysis with SEM, XRD and EDS, the results show that weld seam is composed of Fe-riched phase and Cu-riched phase, with a few of α-Fe but a little of Fe-Ni, ε-Cu and Cu0.81Ni0.19 contained in Fe-riched phase, and with much ε-Cu but a little of Cu0.81Ni0.19, α-Fe and FeNi contained in Cu-riched phase. Dendritic Fe-riched phase distributes in the solid solution of Cu-riched phase. The weld seam alloy has a good bond with the base metal. The aim of double sides forming is obtained by single side welding. The mechanical properties test of weld joint presents that tensile strength is up to 367MPa and the hardness of weld alloying zone is 143.8 HV.

Key words: pulse combustion welding rod; vertical weld; microstructure and property